RECENT RESULTS FROM THE LEAD-GLASS-WALL EXPERIMENT

A. Barbaro-Galtieri
Lawrence Berkeley Laboratory
University of California
Berkeley, California 94720

ABSTRACT

Recent results from LGW experiment are discussed. They include: 1) Study of the $\psi \to 2g\gamma \to \gamma + h$ decay mode, accessible through the analysis of the inclusive γ spectrum; 2) the semi-leptonic decay mode of the D's, specifically the K-e correlation; 3) the measurement of $R_{D\bar{D}}$, the cross section over $\sigma_{\mu\mu}$, for D production up to 7.8 GeV; 4) the study of the charmed quark fragmentation function accessible through D meson spectra.

I. INTRODUCTION

In this talk I present recent experimental results of the Lead Glass Wall (LGW) experiment[1] at SPEAR. These results cover unrelated aspects of e^+e^- collisions and are presented in four separate sections.

In Section I we discuss data relevant to direct photon decay of $\psi(3095)$. The hadronic decay of the ψ is expected to proceed through an intermediate state consisting of three color-octet gluons. In addition to this process, QCD also predicts a non-negligible rate for a process in which one of the three gluons is replaced by a photon. This is what we call a direct photon decay. The photon spectrum of 80,000 ψ decays is analyzed and compared with this hypothesis.

Section II deals with the semileptonic decay of the charmed D mesons. In particular, we study the K-e correlations for D mesons produced at different energies in an attempt to separate the $D \to K^*e\nu$ and $D \to Ke\nu$ decay modes. We also summarize all our results on D meson decays.

Section III summarizes the D production cross section in e^+e^- collisions from threshold up to 7.8 GeV. The energy dependence of the D production follows the shape of the observed total hadronic cross section and explains all the structure in the 4 to 4.5 GeV region.

Section IV deals with momentum and energy spectra of the produced D mesons at 7 GeV e^+e^- energy. These distributions are compared with those from π and K production and provide information on the charmed quark fragmentation function.

The data were taken in the Mark I magnetic detector[2] at SPEAR, modified with the addition of a lead glass detector for γ and e identification.[3] The detector is schematically shown in Fig. 1. The charged particle momentum is measured using the information from the spark chambers and two MWPC that surround the beam pipe. K identification is achieved by measuring the time of flight, TOF, between the e^+e^- interaction region and the trigger counters positioned just inside the magnet coil. The flight path varies between 1.5 and 2 meters. The γ energy is measured in the LGW and π-e separation is obtained by studying the shower development in the LGW. For more details see Refs. 2 and 3.

II. DIRECT PHOTON DECAY OF $\psi(3095)$

All the experimental data on the $\psi(3095)$ are successfully explained with the charmonium model[4] which expects the $\psi(3095)$ to be a $c\bar{c}$ bound state. The decay modes of the ψ can be represented by the diagrams of Fig. 2.

Figure 2a represents the leptonic decay of the ψ. For a vector meson the leptonic width has been calculated to be[5]

$$\Gamma(V \to \ell^+\ell^-) = \frac{16\pi\alpha^2 Q^2}{M^2} |\psi(0)|^2 \left(1 + \frac{2m_\ell^2}{M^2}\right)\left(1 - \frac{4m_\ell^2}{M^2}\right)^{\frac{1}{2}} \qquad (1)$$

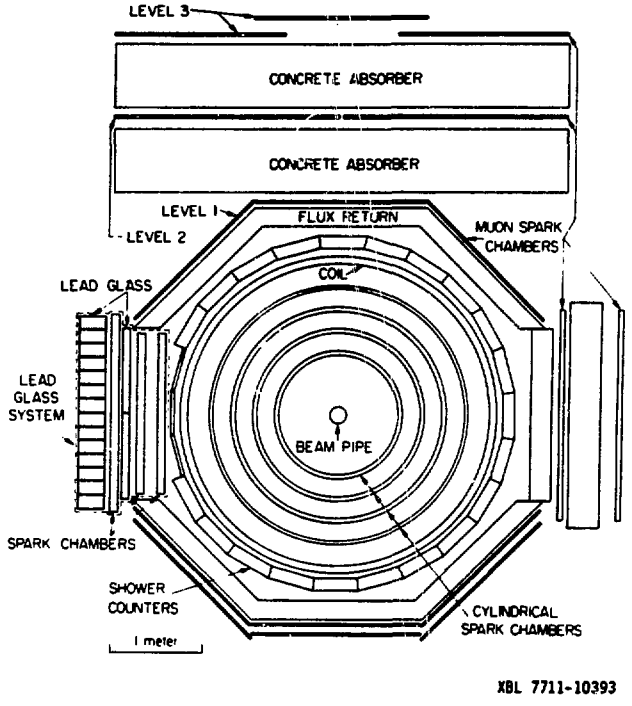

Fig. 1. The SPEAR magnetic detector[2] as seen looking along the beam line. The proportional chambers around the beam pipe and the trigger counters are not shown. The lead glass system (LGW)[3] is shown on the left side of the figure.

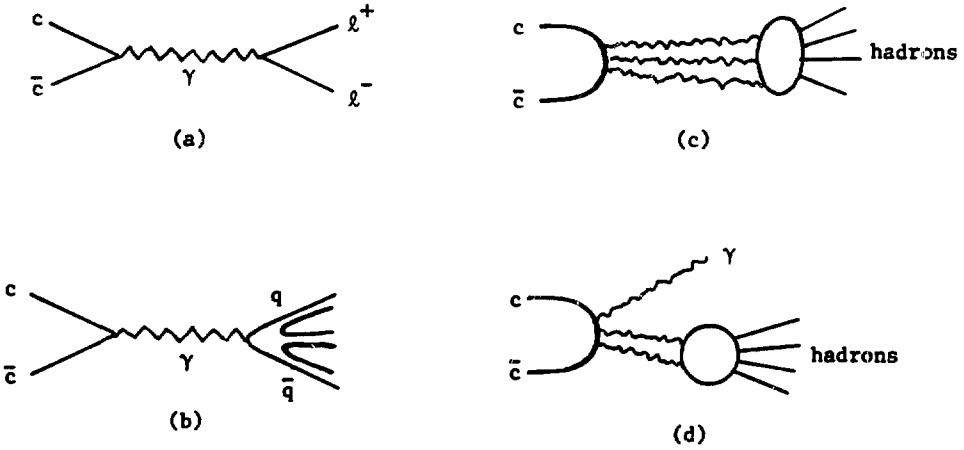

Fig. 2. Schematic diagrams of ψ decays into lepton pairs (a), hadron decays (b) and (c), and direct γ decay (d).

where M is the mass of the vector meson, Q is the charge of the quark, $|\psi(0)|^2$ is the square of the wave function at the origin and m_ℓ is the mass of the lepton. The last two terms become important for decays into $\tau^+\tau^-$ for the more massive vector mesons.

The electromagnetic decay into hadrons can be computed from the diagram of Fig. 2b. In fact, it is

$$\begin{aligned}\Gamma(V \to \gamma \to h) &= 3 \cdot \sum Q_i^2 \cdot \Gamma(V \to e^+e^-) \\ &= R_{back} \cdot \Gamma(V \to e^+e^-)\end{aligned} \tag{2}$$

where the summation is over all types of quarks that can produce hadrons, and 3 is a color factor.

The next two diagrams, 2c and 2d, represent the OZI-forbidden hadronic decays via annihilation into gluons. For the three-gluon decay the width has been derived to be:[6]

$$\Gamma(V \to 3g \to h) = \frac{40}{81\pi}(\pi^2 - 9)\frac{\alpha_s^3}{M^2}|R(0)|^2 \tag{3}$$

where α_s is the running coupling constant of QCD and $|R(0)|^2 = 4\pi|\psi(0)|^2$. The rate for vector meson decay directly into a photon plus hadrons can also be calculated from gluon counting; the result is[7,8]

$$\Gamma(V \to \gamma 2g \to \gamma + h) = \frac{32}{9\pi}(\pi^2 - 9)\frac{\alpha_s^2 \alpha Q^2}{M^2}|R(0)|^2 \tag{4}$$

where all the symbols have already been defined.

The leptonic and hadronic widths of the ψ have been measured,[9,10] but no evidence has been reported yet for the process of Fig. 2d and Eq. (4). The values for Γ_e and Γ_h from Ref. 9 are

$$\Gamma_e = (4.8 \pm 0.6) \text{ keV} \tag{5}$$

$$\Gamma_h = (59 \pm 14) \text{ keV} \quad . \tag{6}$$

From these two measurements and Eqs. (1 - 4) we can derive an expression for the expected fraction of $\psi(3095)$ decay into direct γ + hadrons. Taking the ratio of Eqs. (4) and (3) and doing the necessary algebra we get

$$\frac{\Gamma(\psi \to 2g\gamma)}{\Gamma(\psi \to 3g)} = \frac{0.0234}{\alpha_s} \quad .$$

Next we express $\Gamma(\psi \to 3g)$ as a fraction of the total hadronic decay of the ψ. It is

$$\Gamma(\psi \to h) = \Gamma(\psi \to 3g) + \Gamma(\psi \to 2g\gamma) + \Gamma(\psi \to \gamma \to h)$$

then using the value[9]

$$\Gamma(\psi \to \gamma \to h) = 12 \pm 2 \text{ keV} \tag{8}$$

and Eq. (7) we get:

$$\Gamma(\psi \to 3g) = \Gamma_h \frac{\alpha_s(0.797 \pm 0.059)}{\alpha_s + 0.0234} \tag{9}$$

which leads to the expression

$$\frac{\Gamma(\psi \to 2g\gamma)}{\Gamma(\psi \to h)} = \frac{0.0186 \pm 0.0014}{\alpha_s + 0.0234} \quad . \tag{10}$$

Therefore, the direct γ process of Fig. 2d is inversely proportional to α_s, since α_s is of order 0.2 or larger.

The value of α_s can also be computed from the experimental measurements of Eqs. (5-6), the expressions for Γ_e in Eq. (1), $\Gamma(\psi \to 3g)$ in Eq. (3), and the relation between $\Gamma(\psi \to 3g)$ and Γ_h in Eq. (9). We obtain the following expression for α_s

$$\alpha_s^2(\alpha_s + 0.0234) = 0.00825$$

or

$$\alpha_s(M_\psi) = 0.194 \quad .$$

This value of α_s uses only information on the ψ width. Other analyzes have used information from the whole charmonium spectrum[11] and find values in the $\alpha_s = 0.4$ to 0.5 range. Of course, in order to preserve agreement with the experimental values for Γ_e and Γ_h, higher order QCD corrections will have to be included in the calculated widths.

In conclusion, the expected fraction of hadronic decays into direct γ is dependent upon the value of α_s and, apart from higher order QCD corrections, can be calculated from Eq. (10). We get:

$$B_\gamma = \frac{\Gamma(\psi \to 2g\gamma)}{\Gamma(\psi \to h)} = 8.6\% \quad \text{for } \alpha_s = 0.2 \tag{11}$$

$$= 4.5\% \quad \text{for } \alpha_s = 0.4 \quad . \tag{12}$$

The spectrum of the direct photons has been estimated for massless gluons in Ref. 8. It is expected to increase monotonically as $x \to 1$, where $x = 2P_\gamma/M_\psi$. This characteristic of the spectrum is very important because it allows us to experimentally check the existence of this decay; in fact, the spectrum of γ obtained as decay products of ordinary hadrons is expected to peak at low values of x and decrease monotonically with x. For $\alpha_s = 0.2$ we expect to have a ratio signal/noise = 8/1 for the integrated spectrum at $x > 0.8$.

A. Data Analysis

1. Photon Spectrum. A total of 80,300 events of the type $e^+e^- \to \psi \to$ hadrons were collected in a sample corresponding to an integrated luminosity

of 70 pb^{-1}. The γ's are detected and measured in the LGW (see Fig. 1) which consists of 266 lead glass shower detectors distributed in two layers, the first one (AC) 3.3 X_o thick and the second one (BB) 10.5 X_o thick. In addition, there are three planes of magnetostrictive spark chambers positioned ahead of the system and in between the two layers. These chambers are used to improve on the direction measurement of the γ, as well as to identify the γ's that have converted in the $1X_o$ of Al coil and that need energy correction. For more details, see Refs. 12 and 13.

The energy resolution of the LGW is:

$$\frac{\sigma_E}{E} = \frac{8\%}{\sqrt{E}}$$

where E is in GeV. Figure 3 shows the γ energy measured in the LGW for events of the type $e^+e^- \to \gamma\gamma$ at beam energy $E_b = 1.89$ GeV. The position resolution is

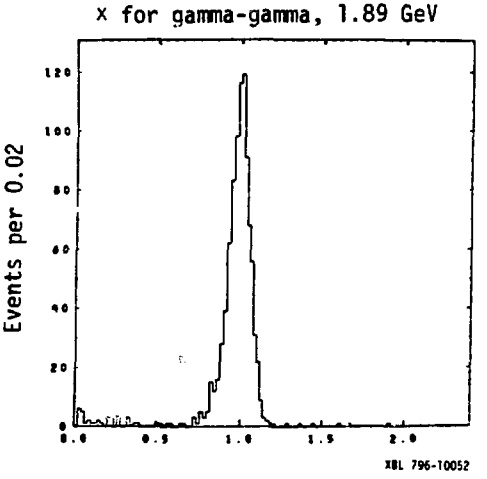

Fig. 3. Ratio of the measured energy over the beam energy for γ rays in the lead glass wall for the reaction $e^+e^- \to \gamma\gamma$. Data are at the $\psi(3772)$; the energy resolution is $\sigma_\gamma/E_\gamma = 5.8\%$.

determined by the size of the lead glass blocks, positioned at a distance between 2.2 and 2.6 meters from the interaction region. The AC are 10.3 cm wide, the BB are 15 cm wide. This information along with the spark chamber measurements provide a resolution: $\sigma = \pm 2$ cm or $\Delta\theta = 0.5°$.

The efficiency for detecting γ's is shown in Fig. 4. Curve 1 shows the efficiency for detecting γ's in the whole system, curve 2 is the efficiency for those γ that have a shower in both the first and second layer of counters. This second category has practically no background and we have chosen this sample for this analysis. The solid angle, after fiducial volume cuts, is 4.9% of 4π.

We normalize the γ spectrum to the total hadronic cross section in order to measure the branching fraction B_γ of Eq. (10). Therefore, we have to know the trigger efficiency and geometrical acceptance of the apparatus as a function of $x_\gamma = P_\gamma/E_b$. The product of the two factors is shown in Fig. 5. It is obtained

Fig. 4. Efficiency for detecting γ rays in the LGW. The curve labeled 1 is the overall efficiency, the curve labeled 2 is for the category of events with the best energy resolution and the least background, that is, for those showers seen in both the AC and the BB.

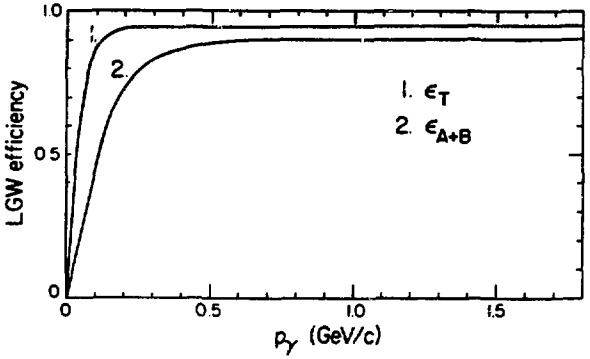

XBL 795-1676

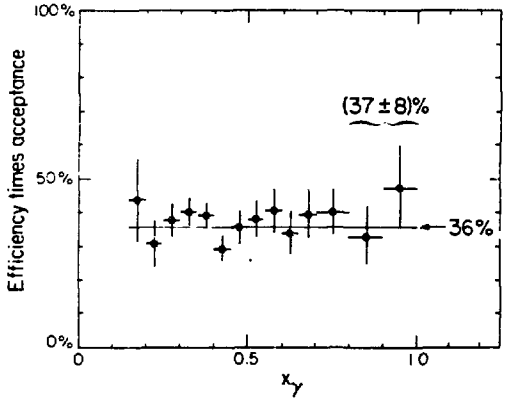

XBL 795-1677

Fig. 5. The total efficiency[13] $\left(\epsilon_{\text{trigger}} \times \text{geometrical acceptance}\right)$ for detecting an event versus $x = E_\gamma/E_b$.

by using the γ converted in the material ahead of the spark chambers ($0.06\ X_o$), so that an e^+e^- pair is detected by the tracking system of the detector. The method is explained in Ref. 13; it provides an efficiency which is model independent and therefore more reliable, although the statistical errors are large.

The γ spectrum thus normalized is shown in Fig. 6 by black dots, the curves in the figure will be explained later. The raw spectrum contains 7020 photons.

In order to detect the process of Eq. (4) we have to evaluate what γ spectrum is expected from the ordinary decay of $\psi \to$ hadrons, since π^0,η and other mesons decay into γ's. To determine the background to direct photon decay we have followed the following procedure:

a) We determine the experimental π^0 spectrum;

b) We compare the π^0 spectrum with the measured $\pi^\pm$ spectrum to verify that they are similar;

c) Since the statistics on the $\pi^\pm$ spectrum are much larger, after step b,

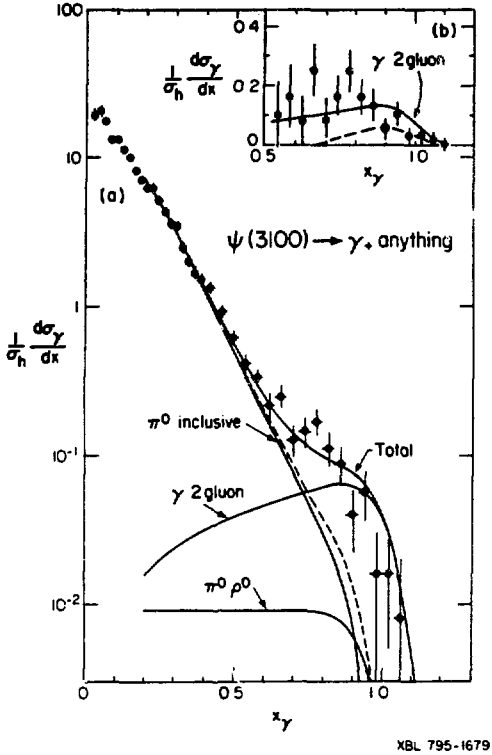

Fig. 6. Inclusive γ spectrum normalized to the total hadronic cross section. The ϕ represents the data in both (a) and (b). (a) The solid lines are labeled, the dashed line is the sum of the "π^0 inclusive" and the "$\pi^0\rho^0$" curves. (b) The γ spectrum shown in (a) after background subtraction (dashed line in (a)). The dashed line represents the contribution to the γ spectrum from ψ decays into $\pi^0\gamma$, $\eta\gamma$, $\eta'\gamma$, $f\gamma$.

we can use the charged π distribution to produce $\pi^0 \to \gamma\gamma$ decay and therefore predict the γ spectrum from this source;

d) Estimate the effect of η decays.

2. Background Determination. Using the events with two or more γ's in the LGW we can study π^0 production. Only γ with momentum $P_\gamma > 100$ MeV/c have been included to eliminate background. The overall efficiency for π^0 detection in the solid angle subtended by the LGW, as a function of momentum, is shown in Fig. 7. The maximum is at 1.4 - 1.5 GeV/c, which is also the maximum momentum that a π^0 can have from ψ decay into hadrons. All the possible γγ invariant masses are constructed and background is subtracted under the π^0 peak. This background is estimated by combining γ pairs where each γ is from a different event. The invariant mass distribution obtained for $P_{\gamma\gamma} > 0.6$ GeV/c is shown in Fig. 8, the background is represented by the smooth curve. The background is smaller at larger P values. This is clearly seen in Fig. 9, which shows the $M_{\gamma\gamma}$ distribution for pairs with $P_{\gamma\gamma} > 1$ GeV. The π^0 spectrum, corrected for LGW efficiency as well as for trigger efficiency and acceptance of the apparatus is shown in Fig. 10. It includes a total of 276 π^0's.

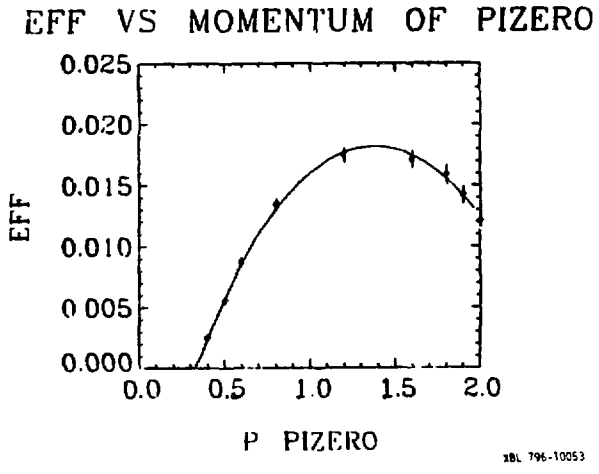

Fig. 7. Detection efficiency for π^0 versus π^0 momentum in GeV/c. The solid angle factors are included.

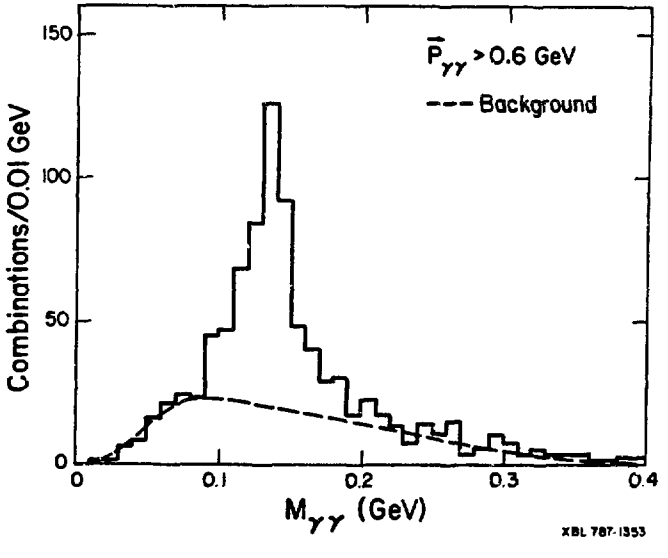

Fig. 8. The $\gamma\gamma$ invariant mass for events with $P_{\gamma\gamma} > 0.6$ GeV/c. The background under the π^0 peak has been calculated by combining γ from different events.

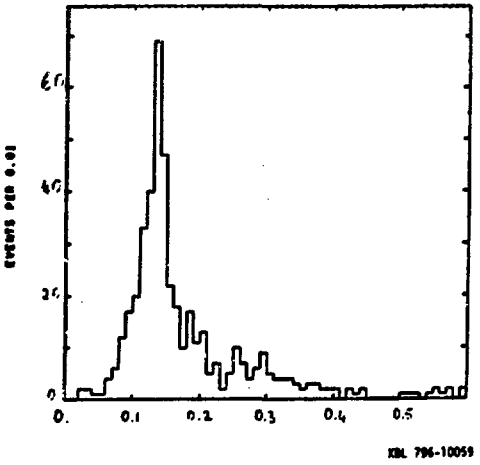

Fig. 9. The $\gamma\gamma$ invariant mass for events with $P_{\gamma\gamma} > 1$ GeV. The resolution of the distribution is $\sigma = 15$ MeV.

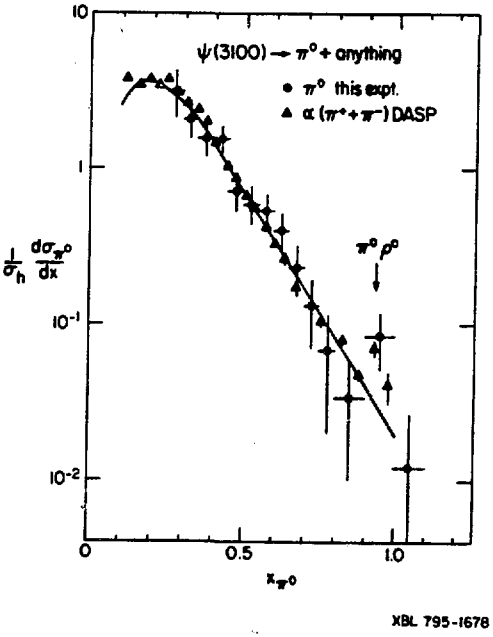

Fig. 10. The dots represent the π^0 inclusive spectrum measured[13] in the LGW at the $\psi(3100)$. The triangles represent the DASP charged π spectrum normalized to the LGW π^0 spectrum. The dashed line is an eyeball fit of the charged π spectrum.

Next we have to compare this spectrum to the charged $\pi^{\pm}$ spectrum. The Mark I detector has K-π-p separation only for $P_K < 0.9$ GeV/c and $P_p < 1.8$ GeV/c, therefore the measured charged particle also includes K and p. The DASP collaboration has reported the $\pi^{\pm}$ and the charged particle spectra separately.[14] Since our charged particle spectrum agrees (apart from an overall normalization factor) with the one of Ref. 14, we have used the DASP $\pi^{\pm}$ spectrum for the comparison. This spectrum, normalized to our π^0 spectrum, is shown in Fig. 10. The shapes of the $\pi^{\pm}$ spectrum and the π^0 spectrum agree reasonably well. The curve represents a fit to the charged π spectrum. For more details the reader is referred to Ref. 13.

Having established that the charged π's are a good model for the π^0 production, we use the curve of Fig. 10 to predict the γ spectrum from π^0 decays. The curve so calculated, normalized to the region of $0.2 < x < 0.4$ is shown in Fig. 6, labelled "π^0 inclusive." It clearly leaves some excess of events at large values of x_γ. The dashed curve is the sum of the "π^0 inclusive" and the $\psi \to \pi^0\rho^0$ curves.

As for η production, very little information is available. In this experiment the solid angle is too small to detect η's and no other measurements have been reported so far. If some η's were produced with the same momentum distribution as the π^0's, the resulting γ spectrum would be softer than that from π^0. The presence of η's would have the effect of increasing the slope of the γ expected from hadronic decays, thus increasing the excess at high x.

B. Results

We have calculated the background for ordinary hadronic decays to the best of our knowledge. Figure 6 shows an excess of events at high x. The expected γ spectrum from the decay mode $\psi \to \pi^0\rho^0$, which is $(1.2 \pm 0.2)\%$ of all the ψ decays[15] is not sufficient to explain the excess. We have made a maximum likelihood fit of the data to the sum of π^0 inclusive, $\pi^0\rho^0$ and $\psi \to 2g\gamma$ processes. The fit obtained is the curve labeled "total" in Fig. 6. After correction for a $(1+\cos^2\theta)$ angular distribution,[8] we obtain

$$B_\gamma = \frac{\Gamma(\psi \to 2g\gamma)}{\Gamma(\psi \to h)} = (4.9 \pm 0.7)\% \qquad (13)$$

to which a systematic error of ±1.3% should be added. This corresponds to a value of α_s

$$\alpha_s = 0.35 \pm 0.12 \qquad (14)$$

where the systematic error is included.

Figure 6b shows the spectrum of γ after background subtraction for $x > 0.5$ with the fitted curve for $\psi \to 2g\gamma$. If we just take the excess of events for $x > 0.6$, without a fit we obtain

$$B_\gamma = (2.7 \pm 0.4)\% \quad \text{for} \quad x > 0.6$$

where the systematic error is now ±0.7%.

Can these events have a source other than the direct γ decay? We have considered two alternatives: 1) *Misidentified* π^0. As mentioned earlier, the position resolution of the LGW system is $\Delta\theta = 0.5°$. The opening angle of the two γ's for a 1.5 GeV/c π^0 is 15°, which, according to Monte Carlo calculation, allows us to separate the two showers. 2) *Other direct* γ *processes*. Four different decay modes involving γ's have been measured and summarized in Table 1. These represent 0.54% of all the ψ decays, or 0.63% of the hadronic decays. With our resolution these decay modes produce a spectrum like the

TABLE 1. Measured branching fractions for $\psi \to \gamma +$ meson decay modes.

Mode	Branching Fraction	Reference
$\psi \to \pi^0\gamma$	$(0.0075 \pm 0.0048)\%$	16
$\psi \to \eta\gamma$	$(0.083 \pm 0.012)\%$	17
$\psi \to \eta'\gamma$	$(0.254 \pm 0.059)\%$	18
$\psi \to f\gamma$	$(0.20 \pm 0.07)\%$	19

dashed line of Fig. 6b, not enough to explain the excess. However, these processes can originate from a diagram such as that of Fig. 2d, where the two gluons produce a π^0, η, η' or f.

In conclusion, we have analyzed our γ spectrum and found an excess of events at large values of x. This excess is consistent with what is expected from the QED process $\psi \to 2g\gamma \to$ hadrons for a value of $\alpha_s = 0.35$. However, we cannot prove that the excess is exclusively due to this process.

III. D MESON DECAY PROPERTIES

In this section we discuss the semileptonic decay mode of the D mesons and a possible method to measure the branching ratio

$$r = \frac{\Gamma(D \to Ke\nu)}{\Gamma(D \to K^*e\nu)} \quad . \tag{15}$$

In addition we summarize the information on D decays obtained in the LGW experiment.

A. Semileptonic Decays of the D Mesons

Some of the Cabibbo favored decay modes of the D mesons are shown in the diagrams below:

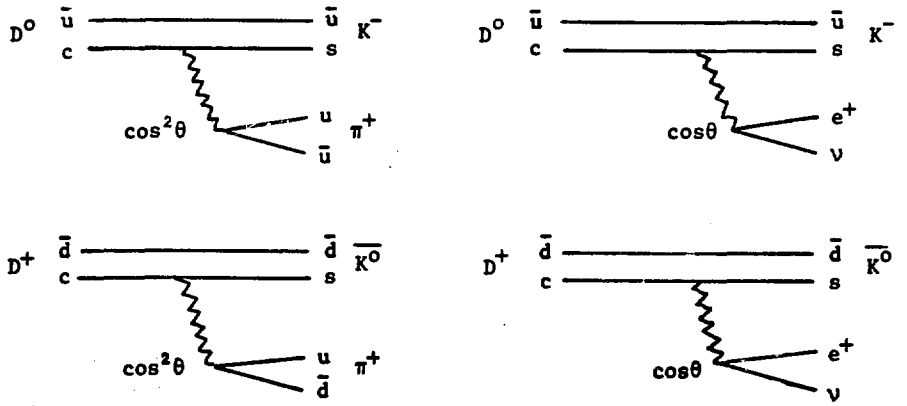

where θ is the Cabibbo angle and the amplitudes for each diagram are proportional to $\cos\theta$ or $\cos^2\theta$ factors as shown. The favored semileptonic decays are:

$$D^0 \to K^- e^+ \nu, \quad K^{*-} e^+ \nu, \quad K^- \pi^0 e^+ \nu \ldots \tag{16}$$

$$D^+ \to \bar{K}^0 e^+ \nu, \quad \bar{K}^{*0} e^+ \nu, \quad K^- \pi^+ e^+ \nu \ldots \tag{17}$$

and charge conjugate reactions. For both D^0 and D^+ the final state includes an e^+ and a K^- or $\bar{K}^0$. The decays with extra pions are suppressed by phase space considerations and by the fact that the matrix elements vanish in the limit that any of the pions is soft.

The branching ratio of the D semileptonic decay into electrons has been measured by the LGW experiment[20,21] as well as by DASP[22] and DELCO[23] and agree with each other very well. The values are shown in Table II, the average value (excluding the DASP result at 4.03 GeV) for the combined D^0 and D^+ mesons is:

$$B_e = (8.3 \pm 1.1)\% \ . \tag{18}$$

TABLE II. The branching fraction for D semileptonic decay into electrons as measured by various experiments. For E > 4.08 GeV other charmed particles may contribute to the measurement.

E (GeV)	Electron events	Background events	Branching fraction (%)	Reference
3.772	61	25	7.2 ± 2.8	LGW[20]
3.90 - 7.38	448	155	8.2 ± 1.9	LGW[21]
3.99 - 4.08	- [a]	- [a]	8.0 ± 2.0	DASP[22]
3.99 - 5.20	182	27	7.2 ± 2.0	DASP[22]
3.77	238 [b]	- [b]	10 ± 2	DELCO[23]

[a] This determination is not independent of the following one.

[b] The number of events and backgrounds for the most recent analysis of this experiment are not available.

In principle the separation of Keν and K*eν decay modes can be done by studying the electron spectrum. Figure 11 shows the spectra obtained by our experiment for D produced in e^+e^- collisions at three different energies.[21] The data is not sufficient to determine the ratio r of Eq. (15) because of statistics limitations and also because at energies above the $\psi(3772)$ uncertainties in the D momentum spectrum lead to uncertainties in the predicted electron spectrum for the two modes. The $D \to K^* e\nu$ peaks at lower P_e than the $D \to Ke\nu$, the decay $D \to K\pi e\nu$ peaks at even lower P_e. In measuring r the assumption is made that the $D \to K\pi e\nu$ is smaller than the $K^* e\nu$, so that the difference between the $K^* e\nu$ spectrum and the sum of the two is negligible.

A better method for separating the $K^* e\nu$ and Keν decay modes is the study of the Ke invariant mass spectra. It contains more information than the single

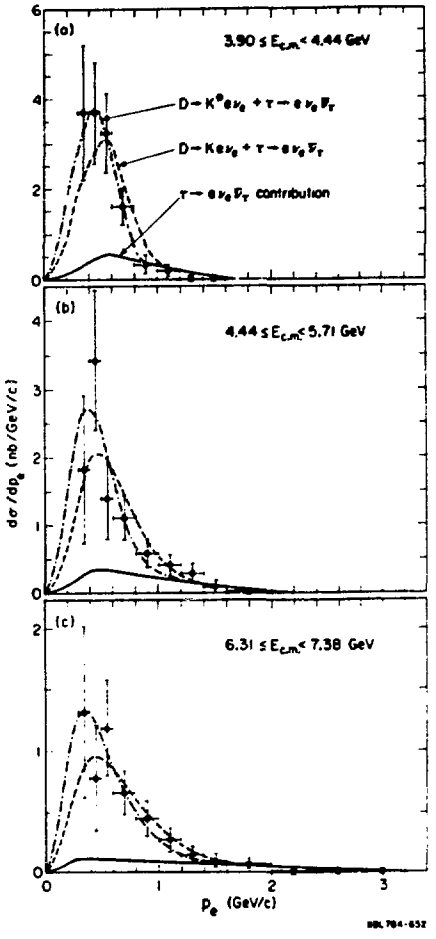

Fig. 11. The momentum spectrum for electrons produced in events with $n_{ch} \geq 3$ in three different energy intervals as obtained by the LGW experiment.[21] The curves are labeled in (a) and the energy intervals are indicated in each graph.

e spectrum, in addition it allows us to combine data from different D momenta, since it is an invariant. Therefore, data obtained at different e^+e^- energy can be combined assuming that the D meson is the source of the Ke pair. Of course, it is necessary to combine the electron with the kaon that comes from the same D, that is, from Eqs. (16,17), the e and the K must have opposite charge. As a consequence the $\overline{K^0}$ modes cannot be used because the $\overline{K^0}$ cannot be distinguished from the K^0. Using only charged K's the Ke spectra include only $K^*e\nu$ for the D^+ and both decay modes for the D^0.

In this experiment the electrons are identified by studying the shower development in the LGW[20,21] and the K by TOF.[24] The Ke invariant mass in four e^+e^- energy intervals[25] are shown in Figs. 12 and 13. The curves represent the spectra expected for the decays $D \to Ke\nu$ and $D \to K^*e\nu$ and each curve was normalized to the observed number of events. All the effects due to acceptance and backgrounds have been included in the Monte Carlo simulation that produced the curves. Each distribution has been fitted to a combination of $Ke\nu$ and $K^*e\nu$ decay modes using a maximum likelihood fit. The results are shown in Table III.

TABLE III. Results of the fits[25] to the Ke invariant mass distributions of Figs. 12 and 13.

E_{CM} interval	Fraction of $Ke\nu$	Fraction of $K^*e\nu$
$\psi(3772)$	0.00 ± 0.12	1.00 ± 0.12
3.90 - 4.44	0.52 ± 0.14	0.48 ± 0.14
4.44 - 5.71	0.83 ± 0.19	0.17 ± 0.19
6.31 - 7.38	0.00 ± 0.04	1.00 ± 0.04

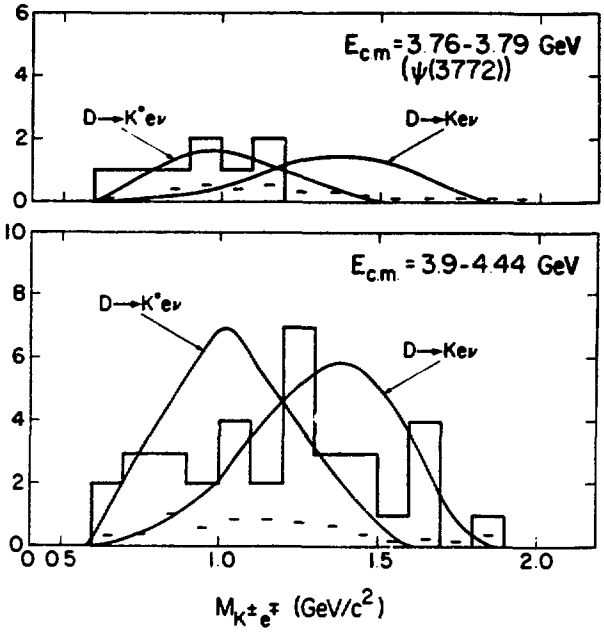

Fig. 12. $K^{\pm}e^{\mp}$ invariant mass spectrum for the ψ(3772) and the 3.90-4.44 GeV regions. The dashed line shows the background from hadrons misidentified as electrons.

XBL 791-298

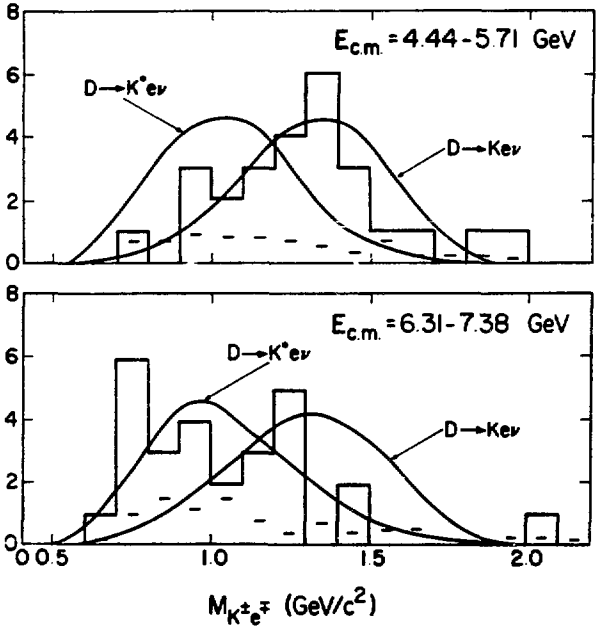

Fig. 13. $K^{\pm}e^{\mp}$ invariant mass spectrum for the E_{CM} = 4.44-5.71 GeV and E_{CM} = 6.31-7.38 GeV regions. The dashed line is the background from hadrons misidentified as electrons.

XBL 791-297

These results seem to indicate that r changes with E_{CM}. Before discussing this effect it is necessary to clarify the relation between r and the fraction of Keν or K*eν we observe. In fact for D^+ only two-thirds of the K*eν events will contribute to the plots of Figs. 12 and 13; for D^0 all Keν and only one-third of K*eν contribute (because only one-third of K^{*-} goes into K^-). Therefore if the $R_p = D^+/D^0$ production ratio changes with energy we expect N_{K^*}/N_K (observed) to change with energy. More precisely the observed ratio is given by:

$$\frac{N_{K^*}}{N_K}\text{(observed)} = \left(\frac{1}{3} + \frac{2}{3} R_p R_d\right) r \qquad (19)$$

where R_d is the ratio of the D^+/D^0 semileptonic decay branching fractions.

One additional effect is due to the fact that there may be contribution to the Ke pairs from other charmed particles like the F meson or, above 5 GeV, charmed baryons. Notice, however, that in Table II the measured branching fractions of semileptonic decays are consistent with no energy dependence, indicating either a small contribution from other charmed particles or that the semileptonic decays are close in values.

We now discuss the results shown in Table III. At the ψ(3772), $R_p \sim 1$ and there are no other charmed particles produced. The K*eν is favored at this energy indicating either that r is large or that R_d is large. At the next two energies the increase in Keν fraction may be due to the observed increase in D^0 production (see Section IV), but then we are at a loss to explain the 6.31-7.38 GeV region where the result seems to be the same as at the ψ(3772), although we know that D^0 is more copiously produced than D^+ (see Section IV).

In conclusion, the method just described may be a good way to measure r of Eq. (15), but it seems to be very difficult to use it with the present data. The problem, apart from statistics, may be due to the presence of charmed particles other than D. Good statistics on the Ke mass spectrum at the ψ(3772) is certainly the best way to measure r.

Recen -esults from the DELCO detector on the electron spectrum[23] at the ψ(3772) are shown in Fig. 14. The curves show the result of a fit to the different decay modes. The

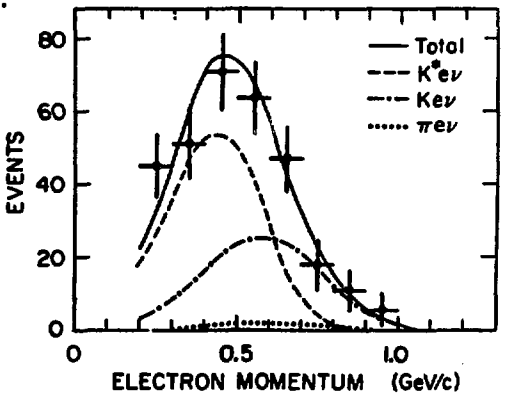

Fig. 14. The electron momentum spectrum from D → eνX as measured by DELCO[23] at the ψ(3772). The curves shown are the result of a fit (see text).

XBL 7812-13696

results are:

$$B(D \to Ke\nu) = (3.7 \pm 2.1)\%$$
$$B(D \to K^*e\nu) = (6.0 \pm 2.3)\%$$
$$B(D \to \pi e\nu) < 2\% \text{ (90\% CL)} ,$$

that is, the $K^*e\nu$ is favored over the $Ke\nu$.

B. Summary of D Decay Modes

In this experiment we have measured exclusive (see Refs. 20,21,24,26) and inclusive[27] decay modes of the D mesons. Table IV summarizes the results of the exclusive measurements done at the $\psi(3772)$.

TABLE IV. Summary of D decay modes and branching fractions measured by the LGW experiment.

Mode	B (%)
$D^o \to K^-\pi^+$	2.2 ± 0.6
$\bar{K}^o\pi^+\pi^-$	4.0 ± 1.3
$K^-\pi^+\pi^-\pi^+$	3.2 ± 1.1
$K^-\pi^+\pi^o$	12 ± 6
$\bar{K}^o\pi^+\pi^-\pi^+\pi^-$	seen
e^+X [a]	7.2 ± 2.6
$D^+ \to \bar{K}^o\pi^+$	1.5 ± 0.6
$K^-\pi^+\pi^+$	3.9 ± 1.0
$\bar{K}^o\pi^+\pi^-\pi^+$	seen
e^+X [a]	7.2 ± 2.6

[a] The quantity measured is an average value for the D^+ and D^o mesons. Here we assume that the two branching fractions are the same.

We note the following:

a) The semileptonic decay is 7.2% (the average of all the experiments is (8.3 ± 1.1)%, Eq. (18)), smaller than expected from quark counting factors alone. In this case we expect,

$$e : \mu : \text{hadrons} = 20\% : 20\% : 60\%$$

instead of 8% : 8% : 84%, which indicates that there is an hadronic enhancement[28] of about a factor 3.

b) Only a small fraction of all hadronic decays have been measured. From Table IV we find

$$\sum_{\substack{\text{measured} \\ \text{modes}}} B_i(D^o \to \text{hadrons}) = (21.4 \pm 6.3)\%$$

$$\sum_{\substack{\text{measured} \\ \text{modes}}} B_i(D^+ \to \text{hadrons}) = (5.4 \pm 1.2)\% .$$

This means that the majority of the decay modes have not been detected yet.

The GIM model[29] predicts that at least 95% of the D decays should include a $\bar{K}$, since the Cabibbo forbidden decays are expected to be ~5%. At the $\psi(3772)$ we have been able to study the inclusive decay of D into K mesons.[27] This was possible because the D's are produced in pairs and no higher mass charmed particle can be produced, so we can use the events of the type $D^0 \to K^-\pi^+$ and $D^+ \to K^-\pi^+\pi^+$ to "tag" the $\overline{D^0}$ and D^- respectively. The results are shown in Table V.

TABLE V. Fraction of charged and neutral kaons in D^0 and D^+ decays.[27]

Mode	Branching Fraction
$D^0 \to K^{\pm}X$	0.35 ± 0.10
$D^0 \to K^0X$	0.57 ± 0.26
$D^+ \to K^-X$	0.10 ± 0.07
$D^+ \to K^+X$	0.06 ± 0.06
$D^+ \to K^0X$	0.39 ± 0.29

We note the following:

a) The total fractions of K per D meson decay are:

$D^0 \to K^{\pm},K^0$	0.92 ± 0.28
$D^+ \to K^{\pm},K^0$	0.55 ± 0.30

not in disagreement within errors with the expected 0.95.

b) For D^0 the K^- and $\overline{K^0}$ decays are, within errors, in agreement with expectations from the statistical model of Quigg and Rosner,[30] which predicts the $\overline{K^0}$ to be more copious than the K^- (52% and 48% respectively).

c) For D^+ the statistical model predicts 33% K^- and 67% $\overline{K^0}$. The measured $D^+ \to K^-$ ratio of 0.10 ± 0.07 seems to be somewhat low. The statistical model as formulated[30] expects a charged multiplicity for D^+ decay of $\langle n_{ch} \rangle = 2.7$, larger than the observed[27] value of $\langle n_{ch} \rangle = 2.3 \pm 0.3$. A reduction of the $\langle n_{ch} \rangle$ in the model tends to reduce the expected fraction of $D^+ \to K^-$ decays from 0.33 down to 0.25. The measured value is still lower than the new estimate and should be measured again with better statistics before drawing any conclusions on this point.

IV. CROSS SECTION FOR D MESON PRODUCTION

We have studied[31] the D meson production cross section as a function of energy in the 3.7 to 7.8 GeV region. The D^+ were identified through the $D^+ \to K^-\pi^+\pi^+$ decay mode, the D^0 through the $D^0 \to K^-\pi^+$ decay mode. The $K^{\pm}$ were identified by TOF, using the weight technique,[33] that is, each particle is assigned a weight proportional to the probability for it to be a π, K or p.

For each particle the weights are normalized to one. The invariant mass for the $K^-\pi^+$ and $K^-\pi^+\pi^+$ combinations are shown in Fig. 15. Clear D signals are

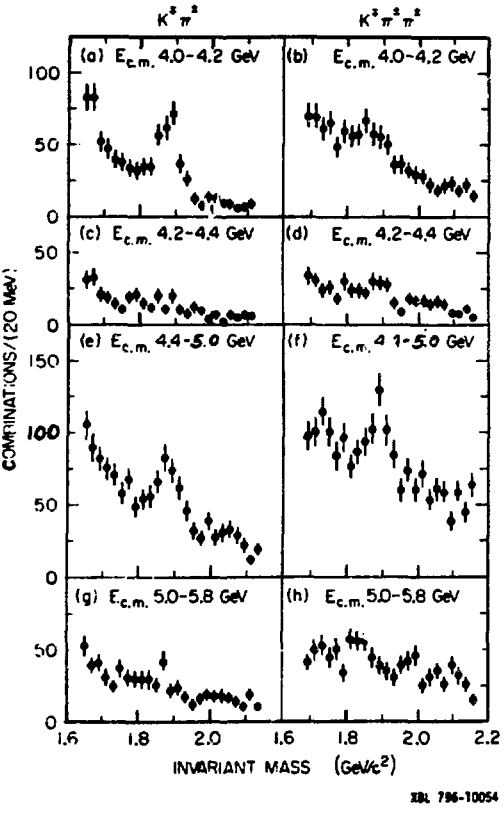

Fig. 15. Invariant mass spectra of weighted $K^\mp\pi^\pm$ and $K^\mp\pi^\pm\pi^\pm$ combinations for several center of mass energy regions.

observed in the intervals 4.0-4.2 GeV and 4.4-5.0 GeV, smaller signals are present at the other energies. The number of D events for each e^+e^- energy interval has been determined by fitting a gaussian superimposed to a smooth background to the data. The results of the fits, along with our results at other energies,[24,34] are shown in Table VI.

The results indicate that the D^+ cross section is systematically lower than the D^o cross section. At the $\psi(3772)$ we expect the $D^o\bar{D}^o$ decay mode to be 56% of the total D production from barrier factors[32] in the Breit-Wigner resonant form due to the D^+-D^o mass difference[24] of 5.0 ± 0.8 MeV. The results are consistent with expectation. At higher energy the effect is larger and is probably due to the fact that a large fraction of the D's are decay products of D^*. The D^*'s decay predominantly into D^o since the D^* and D mass splittings allow $D^{*+} \to D^o\pi^+$ and forbid $D^{*o} \to D^+\pi^-$.

The last column of Table VI shows $R_{D\bar{D}}$, defined as

$$R_{D\bar{D}} = \frac{\sigma_{D^o} + \sigma_{D^+}}{2\sigma_{\mu\mu}} \qquad (20)$$

where the factor two takes into account the fact that a D and $\bar{D}$ are produced in association, either directly or as decay products of D^*. The values of $R_{D\bar{D}}$ are plotted in Fig. 16. They show the same behavior as the total hadronic cross section,[24,35] that is, large production at the $\psi(3772)$ and $\psi(4.03)$ and dips at 3.8 and 4.3 GeV total e^+e^-.

We now compare in detail the D production cross section normalized to $\sigma_{\mu\mu}$,

TABLE VI. Cross sections for D^o and D^+ production at different e^+e^- energies[31] (the charge conjugate states are included, i.e., σ_{Do} means $\sigma_{Do} + \sigma_{\bar{D}\sigma}$). The last column gives the D contribution, $R_{D\bar{D}}$, to the total hadronic cross section expressed as a ratio to $\sigma_{\mu\mu}$.

E Interval (GeV)	$\langle E_{CM} \rangle$ (GeV)	σ_{Do} (nb)	σ_{D^+} (nb)	$R_{D\bar{D}} = \frac{\sigma_{D^+} + \sigma_{Do}}{2\sigma_{\mu\mu}}$
3.73 - 3.76	3.74	< 1.7	< 1.9	< 0.29
3.76 - 3.79[a]	3.775	11.5 ± 2.5	9.1 ± 2.0	1.75 ± 0.27
3.79 - 3.84	3.81	< 0.7	< 0.8	< 0.13
3.84 - 3.89	3.87	2.1 ± 1.4	1.1 ± 1.1	0.28 ± 0.16
4.028[b]	4.03	24.2 ± 7.0	9.6 ± 2.9	3.16 ± 0.73
4.0 - 4.2	4.15	16.5 ± 5.0	6.2 ± 2.5	2.33 ± 0.57
4.2 - 4.4	4.28	3.5 ± 2.1	6.0 ± 2.9	1.03 ± 0.40
4.414[b]	4.41	12.6 ± 4.2	7.8 ± 3.0	2.29 ± 0.60
4.4 - 5.0	4.68	10.9 ± 3.8	10.1 ± 3.5	2.64 ± 0.65
5.0 - 5.8	5.36	5.6 ± 4.4	2.0 ± 2.0	1.26 ± 0.83
6.0 - 7.8[c]	7.0	3.2 ± 0.9	1.7 ± 0.7	1.34 ± 0.33

[a] The D cross sections at this energy, measured in Ref. 32, have been reported by I. Peruzzi et al.[24]

[b] These values are calculated by using the $\sigma \cdot B$ values measured by Piccolo et al[33] and the branching fraction B measured by Peruzzi et al.[24]

[c] From Rapidis et al.[34]

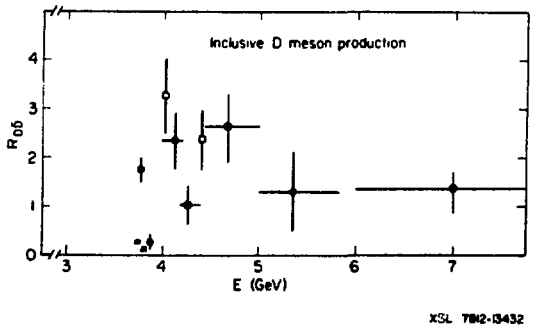

Fig. 16. The cross section for the reaction $e^+e^- \to D\bar{D}$ + anything expressed in units of $\sigma_{\mu\mu}$, $R_{D\bar{D}}$, as a function of energy.[31,24] The solid dots (●) represent the data of the LGW experiment, the squares (□) are calculated from the $\sigma \cdot B$ measurements of Piccolo et al.[33]

Eq. (20), to the expectation for charm production. The total hadronic cross section, that is, $R = \sigma_h/\sigma_{\mu\mu}$ as measured[24,35] in the Mark I detector is shown in Fig. 17. Since there is a high density of points in the figure we have drawn by hand a curve that we can compare with the sum of the different parts that have been measured. This curve is shown in Fig. 18. The individual contribu-

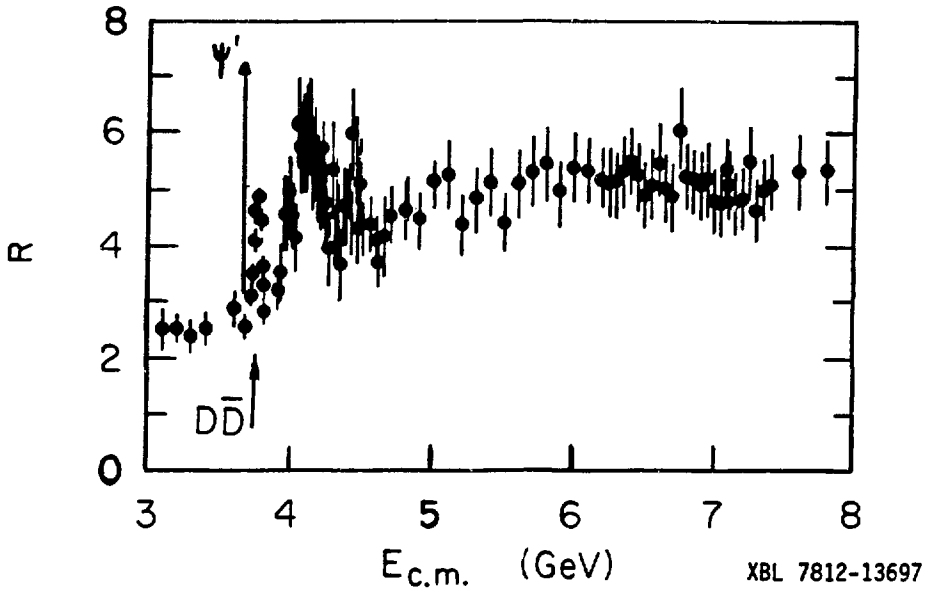

Fig. 17. The ratio of the total hadronic cross section to the μ pair production cross section, $R = \sigma_h/\sigma_{\mu\mu}$, as a function of the center of mass energy. The plot is taken from Ref. 35, the data[24] at the ψ(3772) have been added to it.

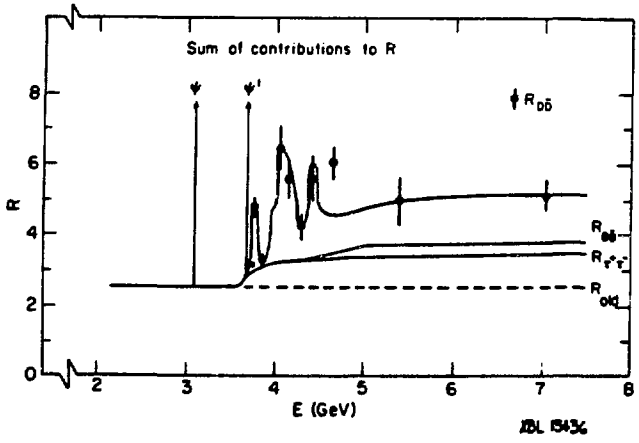

18. A composite graph illustrating the various contributions to R, the total hadronic cross section over $\sigma_{\mu\mu}$. The top curve is a sketch of R, hand drawn over the data of Fig. 17. The following contributions are progressively added starting from R=0; R_{old} is a constant as inferred by the data points below charm threshold; $R_{\tau^+\tau^-}$ is the heavy lepton contribution as calculated from QED; $R_{B\bar{B}}$ is the charmed baryon contribution as inferred by the data of Ref. 36. Finally we add the contribution[31] of $R_{D\bar{D}}$ as data points, taken from Fig. 16 and Table VI.

tions to R were arrived at as follows:

1. These data indicate R = 2.5 below charm threshold, so we will assume that this is the contribution of the old quarks u, d, and s.
2. The heavy lepton contribution to R can be calculated from QED to be $R_{\tau^+\tau^-} = \beta(3-\beta^2)/2$.
3. The charmed baryon contribution to $R_{B\bar{B}}$ has been observed as a step in R with a value that rises from 0 to ½(0.64) = 0.32 between 4.4 and 5 GeV (the $n+\bar{n}$ contribution is assumed to be the same as that of $p+\bar{p}$). Above 5 GeV it is assumed to be constant as indicated by the data of Ref. 36.
4. Finally, the $R_{D\bar{D}}$ values of Fig. 16 and Table VI have been added to the above as points with error bars.

The sum of these contributions appears to saturate the measured values of R. However, the uncertainties of the $R_{B\bar{B}}$ and $R_{D\bar{D}}$ measurements are such that ½ unit of R of F production or some other process could easily be accommodated.

V. D MESON PRODUCTION SPECTRA

There is considerable interest in the dynamical mechanism for fragmentation of heavy quarks into hadrons. The production of D mesons in e^+e^- annihilation provides a clean way for studying the charmed quark fragmentation. For this purpose we have measured[34] the D^+ and D^o spectra at the highest SPEAR energy, in the E_{CM} region of 6 - 7.8 GeV.

The D's are produced in a process that can be schematically represented by the accompanying diagram. In the simplest case just $D\bar{D}$ are produced, more often $D^*\bar{D}^*$, $D\bar{D}^*\pi$, $D\bar{D}^*\pi\pi$, etc. The relevant variable to describe D production are

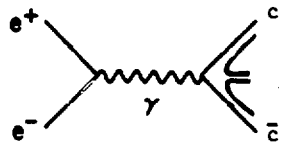

$$x = \frac{2P_D}{E_{CM}} \quad , \qquad z = \frac{2E_D}{E_{CM}}$$

for our E_{CM} region these variables cover the range

$$0 < x < 0.84 \quad \text{and} \quad 0.54 < z < 1 \ .$$

The analysis used a sample of 222,000 hadronic events, corresponding to an integrated luminosity of 22.5 pb^{-1} at an average C.M. energy of 7.0 GeV. The D^o events are selected by taking the appropriate mass region in the $K^-\pi^+$ invariant mass distribution, the D^+ by taking the appropriate region in the $K^-\pi^+\pi^+$ combinations. The K's are identified by TOF as mentioned in Section IV (see Ref. 33). The weighted invariant mass distributions for four bins in z are shown in Fig. 19. The curves are the result of fits of the data to the sum of a gaussian at the expected mass and width of the D and a polynomial background. The numbers of D for each bin that resulted from the fits are shown in the

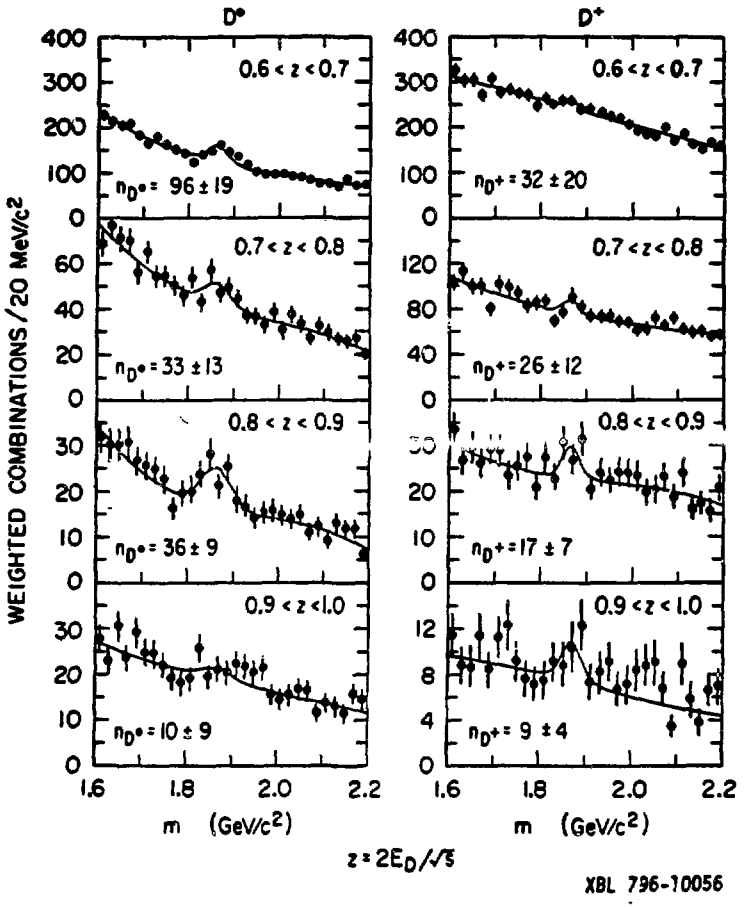

Fig. 19. Weighted invariant mass spectrum for $K^{\mp}\pi^{\pm}$ and $K^{\mp}\pi^{\pm}\pi^{\pm}$ combinations in four different regions of $z = 2E_D/E_{CM}$. The curves are the result of fits (see text).

figure. Similar fits have been made for the distributions in bins of x.

After efficiency corrections and taking into account the known branching ratios[24] (see Section III) for $D^0 \to K^-\pi^+$ and $D^+ \to K^-\pi^+\pi^+$ we obtain the inclusive D spectra shown in Fig. 20. The same spectra are shown in Fig. 21 together with the π and K^0_s inclusive spectra[37,38] for comparison. The D production is similar to the π production and considerably higher than the K^0 production in the z interval 0.6 to 1.0. All three are decreasing functions of z and have approximately the same slope. The γ and π^0 inclusive spectra in e^+e^- annihilation, that we have recently published,[12] also show similar behavior.

There have been many forms proposed for the quark fragmentation function D(z). We have fit the data to some of these forms. For the Feynman and Field

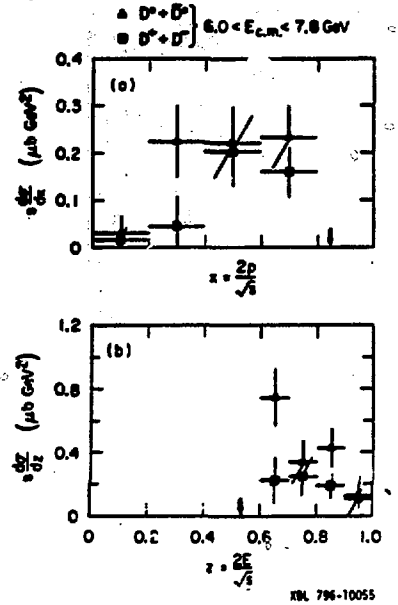

Fig. 20. Inclusive production spectra for charged and neutral D as a function of x and z. The error bars include the relative systematic uncertainties.

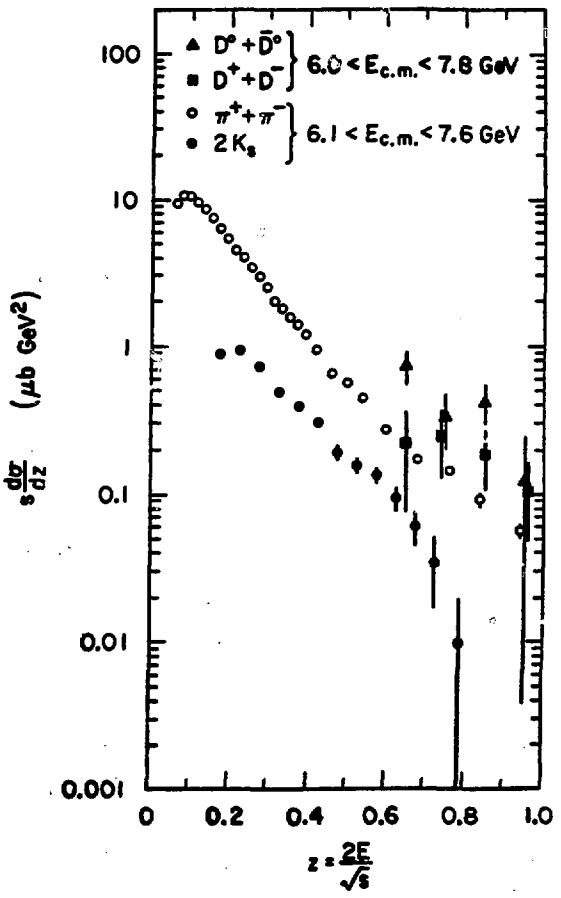

Fig. 21. Inclusive spectra for D^0 and D^+ compared with π and K^0_s spectra from Refs. 37 and 38.

form[39] we have

$$D(z) = \frac{a(1-z)^{\alpha}}{z} \quad , \qquad \alpha = 0.42 \begin{matrix} + 0.28 \\ - 0.23 \end{matrix} \quad . \tag{21}$$

For Gronau et al[40] we have

$$D(z) = b(1-z)^{\beta} \quad , \qquad \beta = 0.63 \begin{matrix} + 0.30 \\ - 0.24 \end{matrix} \quad . \tag{22}$$

Finally for the exponential form[41] we get

$$D(z) = c\, e^{\gamma z} \quad , \qquad \gamma = -3.6 \begin{matrix} + 1.3 \\ - 1.4 \end{matrix} \quad . \tag{23}$$

All of these forms are in reasonable agreement with the data. However, even if the errors are quite large, our data is in disagreement with a D(z) increasing with z. A similar conclusion can be drawn from the D meson spectrum obtained in neutrino reactions.[42]

REFERENCES AND FOOTNOTES

1. The members of the Lead-Glass-Wall collaboration are: A.Barbaro-Galtieri, R.Ely, J.M.Feller, A.Fong, P.Lecomte, R.J.Madaras, T.S.Mast, M.T.Ronan, R.R.Ross, B.Sadoulet, T.G.Trippe, V.Vuillemin (Lawrence Berkeley Laboratory and Dept. of Physics, University of California at Berkeley); J. Dorfan, G.J.Feldman, G.Hanson, J.A.Jaros, B.P.Kwan, A.M.Litke, D.Lüke, J.F.Martin, M.L.Perl, I.Peruzzi, M.Piccolo, T.P.Pun, P.A.Rapidis, D.L.Scharre (Stanford Linear Accelerator Center and Dept. of Physics, Stanford University); B.Gobbi, D.H.Miller (Dept. of Physics & Astronomy, Northwestern University); S.I.Parker, D.E.Yount (Dept. of Physics & Astronomy, University of Hawaii).
2. J.E.Augustin et al., Phys. Rev. Letters 34, 233 (1975).
3. A.Barbaro-Galtieri et al., Phys. Rev. Letters 39, 526 (1977); also J.Feller et al., IEEE Trans. on Nucl. Sci. NS-25, 304 (1978).
4. T.Appelquist and H.D.Politzer, Phys. Rev. Letters 34, 43 (1975). For a recent review article on charmonium models, see T.Appelquist, R.M.Barnett and K.Lane, Ann. Rev. of Nucl. & Part. Sci. 28 (1978).
5. R.Van Royen and V.F.Weisskopf, Nuovo Cimento 50A, 617 (1967), and Nuovo Cimento 51A, 583 (1967).
6. T.Appelquist and H.D.Politzer, Ref. 1.
7. T.Appelquist, A.DeRujula, H.D.Politzer, and S.L.Glashow, Phys. Rev. Lett. 34, 365 (1975). M.Chanowitz, Phys. Rev. D12, 918 (1975). L.Okun, M.Voloshin, ITEP-95-1976.
8. S.J.Brodsky, D.G.Coyne, T.A.DeGrand, and R.R.Horgan, Phys. Letters 73B, 203 (1978).
9. A.M.Boyarski et al., Phys. Rev. Letters 34, 1357 (1975).
10. R.Baldini-Celio et al., Phys. Lett. 58B, 471 (1975). B.Esposito et al., Lett. al Nuovo Cimento 14, 73 (1975).
11. See, for example, the review by J.D.Jackson, C.Quigg, and J.L.Rosner, Proceedings of the XIX Intn'l. Conference on High Energy Physics, August 1978, Tokyo, Japan, p.391 (1978).
12. D.L.Scharre et al., Phys. Rev. Letters 41, 1005 (1978).
13. M.T.Ronan, T.G.Trippe et al., in "The γ spectrum at the $\psi(3095)$," Lawrence Berkeley Laboratory Report LBL-9256 (to be published, 1979).

14. W.Braunschweig et al., Phys. Lett. 63B, 115 (1976) .

15. This is an average value of many experiments. For references, see Particle Data Group, C.Bricman et al., Phys. Lett 75B, 1 (1978).

16. W.Braunschweig et al., Phys. Lett. 67B, 243 (1977).

17. W.Bartel et al., Phys. Lett. 66B, 489 (1977). See also S.Yamada, Proceedings of the 1977 Int. Symposium on Lepton and Photon Interactions at High Energy, Hamburg, August 1977, (DESY, Hamburg, 1977), p.47.

18. W.Bartel et al., Phys. Lett. 64B, 483 (1976). Also S.Yamada, Ref. 17.

19. G.Alexander et al., Phys. Lett. 72B, 493 (1978).

20. J.M.Feller et al., Phys. Rev. Lett. 40, 274 (1978).

21. J.M.Feller et al., Phys. Rev. Lett. 40, 1677 (1978).

22. R.Brandelik et al., Phys. Lett. 70B, 387 (1978). See updated values of the branching fraction in P.H.Wiik and G.Wolf, "A review of the e^+e^- interactions," DESY Report DESY-78/23 (1978).

23. W.Bacino et al., Phys. Rev. Lett. 40, 671 (1977); also J.Kirkby, Proceedings of the 1977 Int. Symposium on Lepton and Photon Interactions at High Energy, Hamburg, August 1977 (DESY, Hamburg, 1977), p.3. See also J.Kirkby, Proc. of the 1978 Summer Institute on Particle Physics, SLAC, 1978, also published as SLAC-PUB-2231 (1978).

24. I.Peruzzi et al., Phys. Rev. Lett. 39, 1301 (1977).

25. J.Feller, "Electrons and Kaons in Charmed Particle Decays," Ph.D. Thesis, Lawrence Berkeley Laboratory Report LBL-9017 (1979).

26. D.L.Scharre et al., Phys. Rev. Lett. 40, 74 (1978).

27. V.Vuillemin et al., Phys. Rev. Lett. 41, 1149 (1978).

28. For a recent review of our results on the D decays relevant to nonleptonic enhancement and for the theoretical references, see: A.Barbaro-Galtieri, "Production and Decay of Charmed Particles in e^+e^- Annihilation," Lectures at the 1978 Erice Summer School, also LBL-8537 (1978).

29. S.L.Glashow, U.Iliopoulos and L.Maiani, Phys. Rev. D2, 1285 (1970).

30. E.Quigg and J.L.Rosner, Phys. Rev. D17, 239 (1978).

31. M.Piccolo et al., "Inclusive K and D Production in e^+e^- Annihilation," LBL Report LBL-7935 and SLAC-PUB-2323 (submitted for publication, 1979).

32. P.A.Rapidis et al., Phys. Rev. Letters 39, 526 (1977).

33. M.Piccolo et al., Phys. Letters 70B, 260 (1977).

34. P.A.Rapidis et al., "Inclusive production of D mesons in e^+e^- Annihilation at 7 GeV," LBL-8143 and SLAC-PUB-2184 (submitted for publication, 1979).

35. R.F.Schwitters, Proc. 1975 Int. Symposium on Lepton Photon Interaction at High Energies, Stanford, California, p.355 (1975).

36. M.Piccolo et al., Phys. Rev. Letters 39, 1503 (1977).

37. V.Lüth et al., Phys. Rev. Letters 70B, 120 (1977); V.Lüth in Proceedings of the Summer Institute on Particle Physics, SLAC, 1977, edited by M.C.Zipf, SLAC Report No. 204.

38. G.Hanson in Proceedings of the 13th Rencontre de Moriond on High Energy Leptonic Interactions and High Energy Hadronic Interactions, Les Arcs, Savoie, France, 1978, edited by Tran Tranh Van, Vol. II, p.15. Also, SLAC-LBL SPEAR Magnetic Detector Collaboration, unpublished data.

39. R.D.Field and R.P.Feynman, Phys. Rev. D15, 2590 (1977).

40. M.Gronau et al., Nucl. Phys. B123, 47 (1977).

41. V.Barger, T.Gottschalk and R.J.N.Phillips, Phys. Lett. 70B, 51 (1977).

42. C.Baltay et al., Phys. Rev. Letters 41, 73 (1978).